Journal of Applied Polymer Science

The Kinetics of Poly(butylene succinate) Synthesis and the Influence of Molar Mass on Its Thermal Properties

Matthieu Garin,[1] Lan Tighzert,[1] Isabelle Vroman,[1] Sinisa Marinkovic,[2] Boris Estrine[2]

[1]Laboratoire d'Ingénierie et Sciences des Matériaux (LISM-EA4695) – Ecole Supérieure d'Ingénieur de Reims, Esplanade Roland Garros, Pôle Henri Farman, 51686 Reims Cedex 2, France

[2]Agro-Industries Recherches et Développements (ARD), Route de Bazancourt, 51110 Pomacle, France

Correspondence to: M. Garin (E-mail: matthieu.garin8@gmail.com)

ABSTRACT: The synthesis of poly(butylene succinate) (PBS) of M_w ranging from 4000 to 180,000 g mol^{-1} is realized with molar ratios $[COOH]_0/[OH]_0$ of 1 and 0.98, and varying amounts of titanium (IV) tetrabutoxide (TBT) catalyst. Polycondensation kinetics are followed by chemical titration of carboxylic groups, and the kinetic rate constants of self-catalyzed and external-catalyzed reactions are calculated. The synthesis of PBS with high molar mass follows the classical Flory theory. The effect of molar mass on PBS thermal properties is also studied. A faster crystallization rate and a higher temperature of crystallization are observed, for very high molar masses. This behavior could be due to a memory effect of the polymer. Complex melting behavior of PBS is induced by a continuous reorganization of the crystalline phase, as observed by MTDSC. DSC measurements also reveal that the crystallinity—and so the amorphous phase—is limited to about 35% when the molar mass M_n is higher than 40,000 g mol^{-1}. © 2014 Wiley Periodicals, Inc. J. Appl. Polym. Sci. **2014**, *131*, 40639.

KEYWORDS: Biopolymers & renewable polymers; differential scanning calorimetry (DSC); polycondensation; thermal properties

Received 3 December 2013; accepted 25 February 2014

DOI: 10.1002/app.40639

INTRODUCTION

According to the European trade association PlasticsEurope, the world production of plastic materials reached about 280 Mt in 2011.[1] And according to the association European Bioplastics, the production capacity of biodegradable and biosourced plastics reached 0.49 and 0.68 Mt, respectively.[2] Although this market share may appear relatively small at first glance, biodegradable polymers have significant potential in three principal sectors: medicine, packaging, and agriculture.[3,4] Biodegradable polymers can be divided into two broad categories.[5] The first, agro-polymers, refers to polymers extracted directly from biomass like polysaccharides, proteins or polyphenols. The second is mostly composed of polyesters generated from conventional chemical synthesis techniques, such as polycondensation and ring-opening polymerization (ROP), or from microbial synthesis. The most recognized and well-studied example of these biodegradable polyesters is poly(lactic acid) (PLA). The chemistry of PLA involves the processing and polymerization of lactic acid (LA) monomer, which is mainly produced commercially by fermentation.[6] Commonly, PLA is synthesized by direct polycondensation polymerization of LA or by ring opening polymerization of lactide, the cyclic dimer of lactic acid.[7–10] Succinic acid (SA) is another alternative in the production of bio-based monomers. With an expected global market estimated at $836.2 million by the end of 2018,[11] SA is a "building block" molecule of great interest in a number of applications, including in the fabrication of antifreeze liquid, solvents, pigments and in the production of poly(butylene succinate) (PBS).[12,13] PBS exhibits balanced performances in thermal and mechanical properties, as well as in thermoplastics processability, compared to other common polymers. Moreover, PBS is one of the most interesting biodegradable aliphatic polyesters because of its melting point (roughly 115°C), which is relatively low compared to aromatic polyesters, and relatively high compared to other aliphatic polyesters.

Many studies have reported on the polymerization of PBS or other poly(alkylene succinate)s. A few researchers have proposed kinetic models for the synthesis of PBS oligomers[14] and two other poly(alkylene succinate)s: poly(ethylene succinate) (PES) and poly(propylene succinate) (PPS).[15,16] A kinetic model was reported for the esterification of poly((butylene succinate-*co*-butylene terephthalate)) (PBST).[17] However, all these studies reported a low molar mass of the final product. More recently, the efficiency of organometal- and metal oxide-based catalysts has been highlighted for the transesterification step of the

Additional Supporting Information may be found in the online version of this article.

synthesis of PBS.[18] Luo et al.[19] proposed a catalytic reaction mechanism for the complex reaction of PBST with high molar masses. Moreover, several authors[20–23] have reported the synthesis of PBS with high molar mass (up to $M_n = 70{,}000$ g mol^{-1}) through the direct polycondensation of SA and 1,4-butanediol (BDO). However, no information was given about polymerization kinetics.

The crystallization and complex melting behavior of PBS, under isothermal and non-isothermal conditions, have been described in the literature for low or high molar masses.[24–29] There are only two articles which offer an explanation for the relationship between M_w and thermal properties.[30,31] The authors compared three different molar mass samples and suggested that the rate of recrystallization decreased with increasing molar mass. Moreover, they assumed that PBS melting and crystallization temperatures, T_m and T_c, respectively, increased with molar mass in the low molar mass region, and decrease in the high molar mass region due to the effect of entanglements. Generally, random introduction of a comonomer unit, such as ethylene succinate,[22] diethylene glycol succinate,[32] butylene terephthalate,[33] propylene succinate,[34–36] or butylene adipate,[37,38] during the synthesis of PBS, decreases both melting point and crystallinity of the copolymer. Recently, Ye et al.[39] reported that the introduction of butylene fumarate increased the melting point of the copolymer while melting enthalpy hardly changed. This behavior was due to a strict isomorphism between butylene succinate and butylene fumarate units. It was also shown that the addition of mica particles into PBS matrix acted as nucleation agents to promote the process of nucleation, while also acted as physical impediments to retard the growth of crystal.[40]

The first phase of this study was to fully characterize the synthesis of high molar mass PBS, by investigating the kinetics of the direct polycondensation between succinic acid and 1,4-butanediol at varying molar ratios of SA/BDO and titanium (IV) tetrabutoxide (TBT) catalyst. The syntheses were followed by acid titration in order to estimate the kinetic rate constants. In the second phase, we studied the crystallization, glass transition and melting of a wide M_w range of PBSs. Melting of PBS was studied by conventional DSC and Temperature Modulated DSC measurements. To our knowledge, this is the first study to examine the dependence of thermal properties on the molar mass of PBS.

EXPERIMENTAL

Materials

1,4-butanediol (BDO) (99%), succinic acid (SA) (99%), titanium (IV) butoxide (TBT) (97%), and chloroform solvent (99.8%) were purchased from Sigma-Aldrich and used without further purification.

Synthesis of PBS

A total of 0.15 mol of SA and desired amounts of BDO and TBT were charged in a 250 mL glass reactor equipped with a mechanical stirrer, a nitrogen inlet and a Dean–Stark (D–S) apparatus with a condenser. The apparatus was immersed in a silicon oil bath and initially heated from 120 to 200°C for 1 h under nitrogen atmosphere to limit the evaporation of BDO during the formation of the first oligomers. Then, a temperature of 200°C was applied for 1 h under nitrogen atmosphere. In the second step of the reaction, vacuum was gradually applied over a 20 min time period, after which the temperature was maintained at 200°C for 2 h. Finally, the temperature was raised to 220°C to increase the molar mass of the resulting PBS. To obtain the reaction rate, samples were taken every 30 min and analyzed by SEC and chemical titration.

Techniques

Size Exclusion Chromatography (SEC). Molar masses of polymers were obtained by SEC, using a Waters HPLC system equipped with a Waters 600 HPLC pump, a Waters 710plus automated injector, a Jasco CO-965 column oven, a Waters 410 Refractive Index (RI) detector and a set of two PLgel 5 μm MIXED-D columns 300 × 7.5 mm. Chloroform was used as eluent at a flow rate of 1 mL min^{-1}, and an approximate sample concentration of 1.5 mg mL^{-1} was used. Polystyrene standards were employed for the calibration curve. The oven and the RI cell temperature were set at 35°C. Samples were filtered through a 0.45 μm PTFE membrane prior to be injected.

End-Group Analysis. Carboxyl end-group content of samples was determined by titration. A known mass sample m_s was dissolved in chloroform at 50°C and then titrated with a KOH/methanol solution ($C_{KOH} = 0.05$ mol L^{-1}) in the presence of phenolphthalein as indicator. Thus, the acid concentration C_{COOH} (mol L^{-1}) and the extent of the reaction of COOH groups' p_{COOH} could be calculated according to eqs. (1) and (2):

$$C_{COOH} = C_{KOH} V_{KOH} / m_s \quad (1)$$

$$p_{COOH} = (n_{0,COOH} - C_{COOH} m)/n_{0,COOH} \quad (2)$$

where V_{KOH} is the volume of KOH solution required to titrate a sample of mass m_s, and $n_{0,COOH}$ is the amount of acid functions in the initial reaction mixture of mass m_0 at $t = 0$. Because of the poor solubility of PBS oligomers in chloroform, we started the acid titration 90 min into the reaction. In addition, assumption was made that the majority of the water was formed during the reaction under nitrogen atmosphere. So, m is the mass of the reaction mixture well after the beginning of reaction: $m = m_0$ - $(18 n_w)$, where n_w is the total mole number of H_2O eliminated. As succinic acid is either in stoichiometric ratio with BDO or in ratio 1:1.02, the theoretical total mole number of H_2O eliminated during the reaction is equal to: $n_w = 2 \times n_{0,AS}$, where $n_{0,AS}$ is the initial amount of succinic acid.

Thermal Properties

Samples used for thermal analysis were taken during synthesis for the kinetic study previously mentioned. All samples were purified by a dissolution/precipitation process in chloroform and methanol, respectively. A Netzsch DSC 204F1, calibrated with metal standards (Hg, In, Sn, Bi, Zn), was used for conventional DSC analysis. Samples of about 10 mg were sealed in aluminium crucibles for the tests. PBS samples were first heated at 150°C for 10 min in order to remove any thermal history, and then cooled to −70°C, at a rate of 10°C min^{-1}, to study their crystallization. After completion of cooling, samples were heated at 150°C again at a rate of 10°C min^{-1} in order to study glass

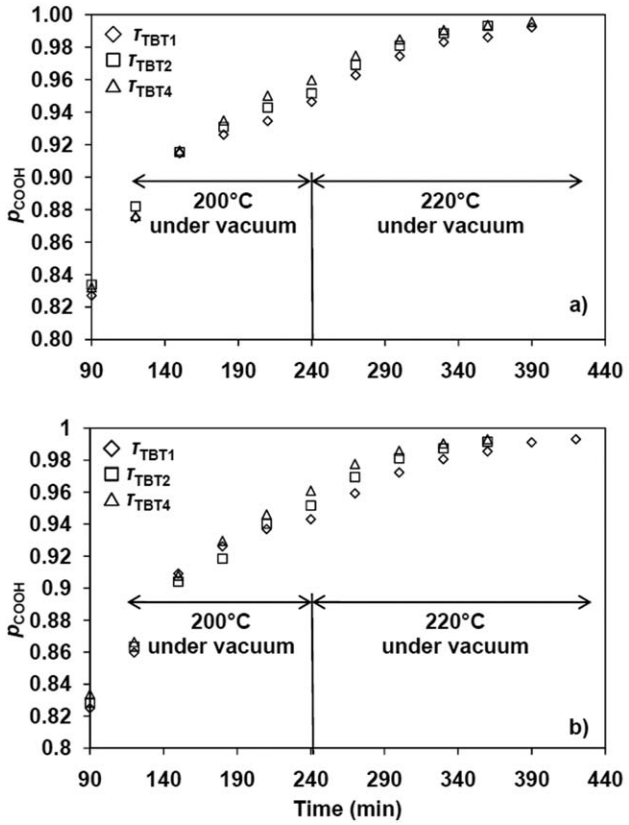

Figure 1. Extent of reaction of COOH groups versus time for (a) $r = 1$ and (b) $r = 0.98$ with three catalyst ratios. p_{COOH} was calculated from eq. (2). The average standard deviation observed in p_{COOH} is 1.10^{-3}.

transition and melting behavior of PBS. All tests were carried out under nitrogen flow.

The second derivative of the DSC signals was selected as the criteria to determine the exothermic and endothermic phenomena which occur in the melting region. Therefore, the DSC curves were fitted with asymmetric Gaussian model to estimate the surface of different events which occur during endotherms. The software "Fityk ver. 0.8.9" was used to fit the curves, and the peak of each resulting asymmetric Gaussian curve was chosen from the peaks of second derivative of the DSC curves. For the Modulated Temperature DSC, we worked under *heat-only* conditions in order to avoid influencing the reorganization effects under investigation during sample melting. In addition, it is recommended that both the underlying heating rate and the oscillations period allow a minimum of 4–6 cycles across the width of the transition studied.[41] Therefore, the thermal phenomena of the samples were studied during the second heating scan with a 1°C min^{-1} underlying heating rate, a 60 s period and a 0.1°C amplitude.

RESULTS AND DISCUSSION

Kinetic Study of the Synthesis of PBS and Influence of Catalyst Concentration

Two different monomer ratios ($r = [COOH]_0/[OH]_0 = 1$ and 0.98) and three different molar ratios of TBT over SA ($\tau_{TBT} = 1$, 2 and 4 mmol/molSA denoted τ_{TBT1}, τ_{TBT2}, and τ_{TBT4}, respectively) were used to study the kinetics of PBS polymerization. For $r = 1$ and $r = 0.98$, the molar mass versus time measurements showed that the higher the ratio of TBT, the faster the increasing molar mass. A maximum of M_w and M_n of 178,800 and 63,600 g mol^{-1}, respectively, were obtained after 6.5 h under the conditions: $r = 1$ and τ_{TBT4}. The evolution of molar mass M_w versus time for each synthesis is given in Supporting Information Figure S1. The polydispersity index (*PDI*) ranged from 1.6 to 2.8. We can note that *PDI* increased as both molar masses M_n and M_w increased.

The extent of the reaction p_{COOH} versus time was followed by acid titration [see eq. (2)] for two monomer ratios and three catalyst ratios. Data shown in Figure 1 correspond to samples obtained after the last 30 min of the reaction under nitrogen atmosphere and the full period under vacuum at 200 and 220°C. At the beginning of reaction, low M_w PBSs are not soluble in chloroform; therefore titration is not possible. All curves start at $p_{COOH} \approx 0.83$ corresponding to 90 min in Figure 1. This clearly indicates that the majority of acid functions are consumed after a reaction time of 90 min. Moreover, catalyst effect on reaction extent can be noted, from 200 min to 340 min, as p_{COOH} increases when τ_{TBT} increases. However, this difference is no longer observable for either τ_{TBT2} or τ_{TBT4} when $p_{COOH} > 0.99$.

It is well-known that diacid monomers have almost no autocatalytic effect when polyesterification is carried out in presence of an external catalyst. Indeed, for a stoichiometric ratio of acid and hydroxyl groups, the degrees of polymerization $\bar{X}_n = f(\sqrt{t})$ and $\bar{X}_n = f(t)$ are linear for self-catalyzed or external-catalyzed reactions, respectively. Titanium compounds such as TBT are sensitive to moisture and can form oligomeric species under hydrolysis conditions.[42] Also, it was reported very recently that titanium tetralkoxides lose their efficiency in the presence of water.[18] However, titanium catalyst deactivation is a much-discussed subject since the oligomeric form of these compounds is still catalytically active.[43,44] Thus, in order to properly evaluate the efficiency of the two catalytic mechanisms (autocalysis and external catalysis), both kinetic models were employed in our systems. In addition, as the kinetics of polyesterification are very sensitive to the monomer ratio *r*, two different kinetic systems were considered, for stoichiometric and non-stoichiometric ratios of functional groups. This study was realized for the under-vacuum reaction part.

Given the relatively low boiling point of BDO (230°C) and its dehydration forming tetrahydrofuran (THF), we analyzed the distillate collected in Dean-Stark apparatus and vacuum trap for one synthesis ($r = 0.98$ and τ_{TBT1}) by ^{1}H NMR. NMR spectra (Supporting Information Figure S2) show that distillate is mainly composed of water ($\delta = 4.9$ ppm). However, we also observed low intensity peaks attributed to methylene groups of BDO ($\delta = 3.6$ and 1.6 ppm) and THF ($\delta = 1.9$ and 3.7 ppm). Thus, we estimated a mixture of water containing around 0.5 and 1.5 mol% of THF and BDO, respectively. The formation of THF and loss of BDO modifies the reaction stoichiometry and can highly reduce the polymerization degree expected. The following kinetics study showed whether these losses influenced the Flory theory.

Table I. Reaction Rate Constants of Both Self-Catalysis (k) and External-Catalysis (k') Models. k and k' are Multiplied by a Factor 10^5 and are Expressed in $kg^2\ mol^{-2}\ s^{-1}$ and $kg\ mol^{-1}\ s^{-1}$, Respectively

	r = 1			r = 0.98		
	200°C		220°C	200°C		220°C
	k	k'	k'	k	k'	k'
τ_{TBT1}	20	14	90	11	10	38
τ_{TBT2}	26	17	-[a]	- [a]	13	56
τ_{TBT4}	- [a]	24	263	- [a]	16	58

[a] Constant values could not be obtained due to the non-linear behavior of plotted data.

First Case: Stoichiometric Ratio of Functional Groups. Flory[45] showed that self-catalyzed polyesterification rate is second-order for diacid and first-order for diol, while the external-catalyzed reaction rate is first-order for both diacid and diol. Therefore, in the case of stoichiometric ratio of the functional groups, the kinetic equation of a self-catalyzed reaction is defined by:

$$1/(1-p)^2 = 2[M]_0^2 kt+1 \quad (3)$$

and the kinetic equation of an external-catalyzed reaction is defined by:

$$1/(1-p) = [M]_0 k' t+1 \quad (4)$$

where $[M]_0$ is the initial concentration of acid or hydroxyl groups and k and k' are kinetic rate constants of the self-catalyzed and the external-catalyzed reactions, respectively. In the case of eq. (4), the activity of external catalyst is a constant included in k'. Equation (3) is generally valid for p ranges from 80 to 93%, while eq. (4) has to be applied with caution for very high extent of reaction ($p > 99\%$).[46] p was calculated with eq. (2) and the plots of both eqs. (3) and (4) can be found in Supporting Information Figures S3 and S4. The first results obtained at 200°C showed clearly that the autocatalytic effect of SA is significant when the two lowest amounts of catalyst τ_{TBT1} and τ_{TBT2} are introduced in the reaction medium. Results obtained at 220°C for the external-catalyzed reaction must be considered with caution. Indeed, an extent of reaction higher than 0.99 is reached for the two amounts τ_{TBT2} and τ_{TBT4}. Moreover, the τ_{TBT2} plot deviates strongly from the linear behavior.

Second Case: Non-Stoichiometric Ratio of Functional Groups. Kinetics of polyesterification are very sensitive to r, so we took into account this ratio for the kinetic models where $r = 0.98$.

Self-Catalyzed Reaction. The reaction rate equation is defined by:

$$-d[\mathrm{COOH}]/dt = k[\mathrm{COOH}]^2[\mathrm{OH}] \quad (5)$$

The complete integration of eq. (5) is given in Supporting Information, and the integrated rate equation Y_1 is obtained:

$$Y_1 = A\left(\frac{1}{[\mathrm{COOH}]} - \frac{1}{[\mathrm{COOH}]_0}\right) + ln\frac{[\mathrm{COOH}]([\mathrm{COOH}]_0 + A)}{[\mathrm{COOH}]_0([\mathrm{COOH}] + A)} = A^2 kt \quad (6)$$

where $A = (1\text{-}r)[\mathrm{OH}]_m$.

External-Catalyzed Reaction

The rate equation is defined by:

$$-d[\mathrm{COOH}]/dt = k'[\mathrm{COOH}][\mathrm{OH}] \quad (7)$$

As for eq. (6), the complete integration of eq. (7) is given in Supporting Information, and the integrated rate equation Y_2 is obtained:

$$Y_2 = \frac{1}{A}\ ln\frac{[\mathrm{COOH}]_0([\mathrm{COOH}] + A)}{[\mathrm{COOH}]([\mathrm{COOH}]_0 + A)} = k't \quad (8)$$

Concentrations of acid functions [COOH] were calculated with eq. (1) and the data of $Y_1 = f(t)$ and $Y_2 = f(t)$ are plotted in Supporting Information Figures S5 and S6. As in the case of stoichiometric ratio, results obtained at 200°C showed an influence of the autocatalytic effect of SA when the polymerization of PBS is carried out with τ_{TBT1}. On the other hand, plotted data at 220°C for an external-catalyzed reaction gave an excellent linear relationship for all τ_{TBT}. Note that in this case, p is almost lower than 0.99 for all τ_{TBT}.

In spite of the relatively high amounts of catalyst introduced in the reaction medium, acid functions of SA play a significant catalytic role in the synthesis of PBS for both τ_{TBT1} and τ_{TBT2} at $r = 1$ and for τ_{TBT1} at $r = 0.98$ when p ranges from around 0.82 to 0.95. Moreover, the external-catalysis model is also adapted for all τ_{TBT} and both r of 1 and 0.98 in the same range of p. This behavior may be explained by the efficiency loss of TBT in the presence of water formed in polyesterification, as has been previously reported in the literature.[18,42] However, we can say that the catalytic activity of TBT is not totally deactivated.

Kinetic rate constants k and k' were calculated from the slope of the linear fitting of the data and are presented in Table I. From these values, it seems that the polymerization of PBS is 2nd order at r of 0.98 for τ_{TBT2} and τ_{TBT4} in the entire studied range of the reaction and for τ_{TBT1} at 220°C, while a contribution of the two catalytic mechanisms should occur for τ_{TBT1} at 200°C.

At $r = 1$, for τ_{TBT1} and τ_{TBT2}, at 200°C linearity observed could evidence a simultaneous contribution of the two catalytic mechanisms, whereas for τ_{TBT4} reaction could be mainly external-catalyzed, thus a 2nd order. At 220°C, the last part of the reaction is 2nd order for τ_{TBT1}. However, for τ_{TBT4}, k' value cannot be considered accurate as $p > 0.99$ (see comments above). Also, k' value for τ_{TBT2} could not be calculated as the plot is not linear (cf. Supporting Information Figure S4). For a given τ_{TBT}, as expected, both k and k' are always higher for $r = 1$ than those of $r = 0.98$ and k' increases as τ_{TBT} increases. These results show that the modification of the reaction stoichiometry (by formation of THF and loss of BDO) did not influence the Flory theory. However, we also observe an unexpected increase in k values with increasing τ_{TBT} for $r = 1$. This behavior may be explained by the synergy between two catalytic mechanisms; the presence of the catalyst TBT may increase the rate of reaction

Table II. Molecular and Crystallization Characteristic Data of PBS Samples used for the Thermal Study

Sample	PBS1	PBS2	PBS3	PBS4	PBS5	PBS6	PBS7	PBS8
M_n (g mol^{-1})	5400	10,000	14,500	29,400	40,000	55,300	59,700	69,300
M_w (g mol^{-1})	9500	17,900	26,000	60,000	96,600	129,000	144,400	158,600
T_c (°C)	73.6	70.4	74.5	70.1	68.6	73.3	86	86.8
$T_{1/2}$ (min)	1.36	1.22	1.28	1.4	1.56	1.42	0.91	1.01
ΔH_c (J g^{-1})	85.1	83	78.5	73.5	68.6	70.3	68.1	70.1
X_c (%)	42.5	41.5	39.3	36.8	34.3	35.1	34.1	35.1

and thus more rapidly decrease the concentration of acid functions.

All synthesized samples were used for further testing, which included extensive thermal behavior characterizations. Authors chose to present resulting data from these testing in the next part of this article.

Thermal Properties

Thermal properties of PBS with different molar masses were characterized by DSC. These measurements were realized with a series of samples, issued from the previously kinetic study, which are given in Table II. In the following discussion, we first present the results for the melt-crystallization of PBS from conventional DSC measurements. Then, we present the results for the melting of PBS from conventional and Modulated Temperature DSC measurements. Finally, we deal with results regarding the glass transition of PBS.

The Melt-Crystallization of PBS. As can be seen in Figure 2, melt-crystallization peaks of the different PBS samples are almost symmetric and take place in a narrow temperature range, which suggests that the formation of crystals is rather homogeneous. However, there is no obvious tendency in the evolution of the crystallization temperature, T_c, for the samples from PBS1 to PBS6 (Table II).

We can note an increase in T_c only for the two samples of greater M_w, PBS7 and PBS8. Under the same cooling-rate conditions, Yasuniwa and Satou[30] measured a T_c of around 75°C for a PBS with a M_w of 110,000 g mol^{-1}, while those for samples with M_w of 180,000 g mol^{-1} and 250,000 g mol^{-1} fell between 80 and 85°C, with a slightly lower T_c for sample with a M_w of 250,000 g mol^{-1}.

They explained this behavior by suggesting that T_c increases with molar mass in the low molar mass region and that T_c decreases in the high molar mass region due to the effect of entanglements.[30] On the one hand, it seems difficult to accept that there are no entanglement effects for samples with M_w as high as 110,000 g mol^{-1} and 180,000 g mol^{-1}. On the other hand, by following this assumption, we should observe a large decrease in T_c for our samples with a very low M_w, which is not the case. Moreover, a T_c (73.8°C) in the same range as our samples was measured by Papageorgiou et al.[25] for a PBS sample with a M_n of 6800 g mol^{-1}.

As can be seen in Table II, we also estimated the time $t_{1/2}$ when the degree of crystallinity reached 50%. As for the values of T_c, there is no apparent tendency in the evolution of $t_{1/2}$ for the samples from PBS1 to PBS6. We note a decrease in $t_{1/2}$ only for the two samples of greater M_w, PBS7 and PBS8. This result suggests that the crystallization rate of samples PBS7 and PBS8 is greater than that of the other samples with lower M_w.

The very different behaviors of these two samples could be explained by polymer memory effects, as has been suggested by Rieger.[47] The term "memory effects" means that a polymer sample may be completely molten (according to calorimetric or rheological data) and still retain partial memory of its former crystalline structure.[47] In our case, we can assume that these memory effects are more present for the samples with the highest molar masses. Indeed, we can easily imagine that the relaxation of these samples—beyond the melting point—is reduced by the significant length of the macromolecules, which has the effect of partially maintaining the precursors for nuclei. The improved preservation of these precursors could explain the greater temperature and rate of crystallization.

Finally, the measurement of the enthalpy of crystallization ΔH_c (Table II) shows that molar mass has a significant influence on the degree of crystallinity X_c of PBS. In considering the enthalpy of crystallization of a 100% crystalline PBS of 200 J g^{-1},[24] we observed a decrease of X_c from about 43 to 35% as M_w increases from 9500 g mol^{-1} to 96,600 g mol^{-1} (Table II). Beyond this, the value X_c remains constant at around 35%. This behavior can be explained by the effect of entanglements on

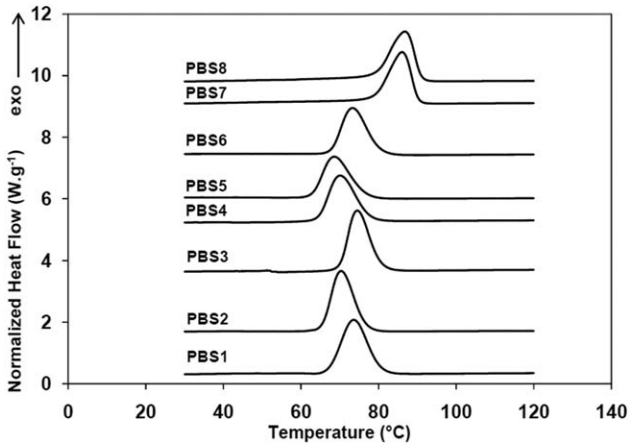

Figure 2. DSC thermograms for PBS samples with various molar masses during non-isothermal crystallization. Cooling rate of 10°C min^{-1}.

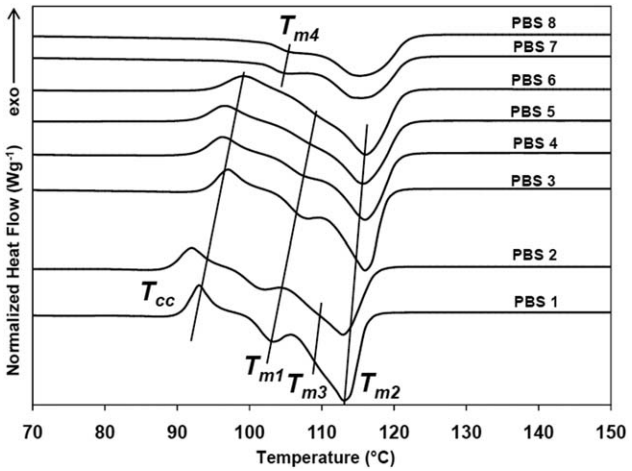

Figure 3. DSC thermograms for PBS samples with various molar masses during fusion (2nd scan). Heating rate of 10°C min^{-1}.

macromolecules movement and so on the process of PBS crystallization.

The Melting of PBS. ***Conventional DSC measurements.*** Thermograms of the melting region of the different PBS samples are grouped in Figure 3. In the following description, T_{m1}, T_{m2}, T_{m3}, and T_{m4} are used to denote the different endotherms and T_{cc} represents the cold-crystallization. ΔH_{m1} and ΔH_{m2} are the enthalpies of fusion assigned to T_{m1} and T_{m2}, respectively. ΔH_{mt} denotes the total heat of fusion and ΔH_{cc} is the enthalpy of cold-crystallization assigned to T_{cc}.

As can be seen, these thermograms can be separated into three groups depending on molar mass. The first group is composed of samples with the lowest molar masses, PBS1 and PBS2. We first observe a cold-crystallization peak T_{cc} around 92°C followed by a first endothermic peak T_{m1} at 103 and 101.5°C for PBS1 and PBS2, respectively. The final melting peak T_{m2} is located at 113°C, which corresponds to the fusion of the last and larger crystals. The second derivative [Figure 4(a)] showed a third endothermic peak T_{m3} located between T_{m1} and T_{m2} at 110 and 109°C for PBS1 and PBS2, respectively. The second group of thermograms is composed of the samples with intermediate molar masses, PBS3 to PBS6. As can be seen, it is the same kind of thermograms as the first group, but with a shift toward higher temperatures.

The first T_{cc} is located at around 96.5°C for the samples PBS3 to PBS5, while that of PBS6 is at 99°C. The temperature of peak T_{m1} remains nearly constant at around 107°C for samples PBS3 to PBS5 and rises to 109°C for PBS6.

The second derivative [Figure 4(b)] shows that peak T_{m3} has disappeared, and there is only the final peak T_{m2} at around 116°C. Finally, the third group is formed by the two samples with the highest molar masses, PBS7 and PBS8. The largest difference between this group and the two previous ones is the disappearance of the cold-crystallization T_{cc} and the appearance of a new endothermic peak T_{m4} located at around 106°C [Figure 4(c)]. The final melting peak is divided into two endotherms corresponding to T_{m1} and T_{m2} at 114 and 117.5°C, respectively.

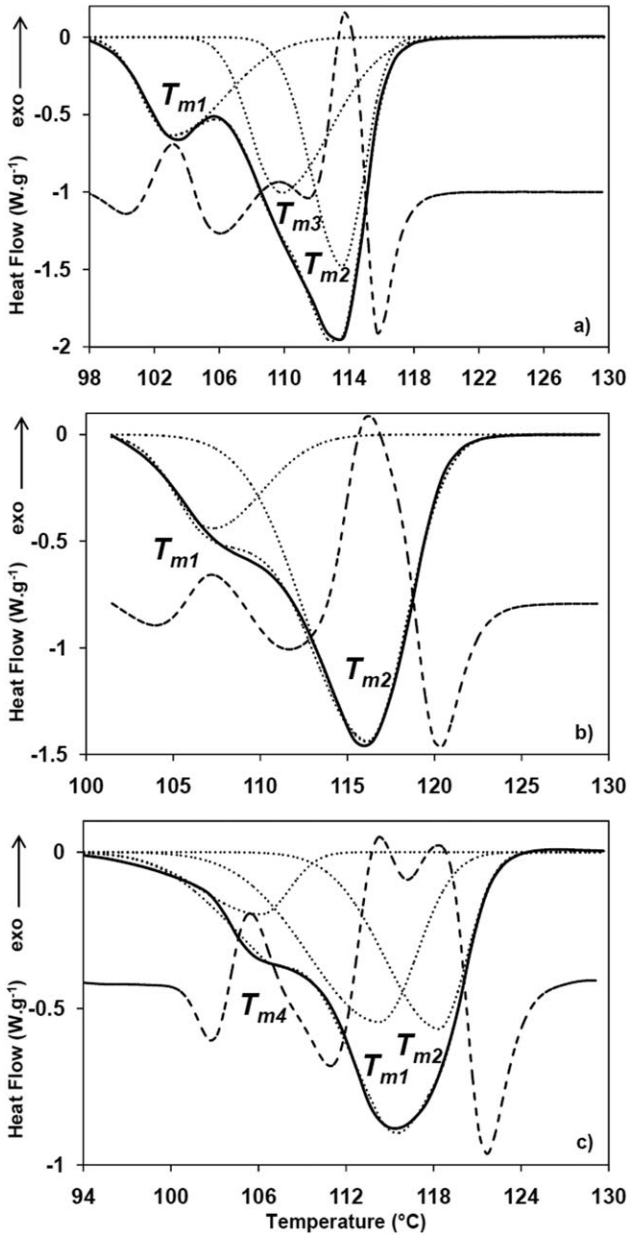

Figure 4. DSC signals (–), second derivatives (– – –) and non linear adjustments (....) of (a) PBS1 as an example of the first thermograms group, (b) PBS5 for the second one, and (c) PBS8 for the third one.

It can already be said that the presence of multiple endotherms is not related to a crystal modification. Indeed, a number of studies[24,26,29] have shown that the crystalline structure of PBS is monoclinic before and after the exothermic peak T_{cc}. Thus, this behavior should be related to a difference in thermal stability between PBS crystals. In other words, there is a crystal size distribution (contrary to what was suggested earlier in the crystallization process). Usually, this complex behavior is interpreted as a melting-recrystallization-melting process. In our case, we only observe a process of crystallization-melting for the first two groups mentioned above, while in the third group we only observe a fusion of the polymer. According to Yasuniwa and Satou,[30] the two first melting-recrystallization steps are due to

the transformation of small and/or imperfect crystals to more stable crystals. This means that there is a competition between the two endothermic and exothermic processes. So, when the rate of crystallization predominates over that of melting, an exothermic peak occurs. And in the opposite case, an endothermic peak appears. Similar behavior has been reported by Yoo and Im.[29]

The evolution of the two enthalpies of fusion ΔH_{m1} and ΔH_{m2} relative to T_{m1} and T_{m2}, respectively, with M_w is presented in Figure 5. As shown, in the presence of the exothermic peak T_{cc}, ΔH_{m2} increases as molar mass increases up to around 150,000 g mol^{-1}, while ΔH_{m1} decreases. For a polymer, the higher the melting point, the more stable the crystals. This means that in the case of our samples, more and more stable crystals are formed until the molar mass reaches about 150,000 g mol^{-1}. Beyond that point, the two enthalpies ΔH_{m1} and ΔH_{m2} are mostly constant, meaning that the amount of the thickest crystals is mostly constant too.

However, we observe an increase of ΔH_{m1} and a decrease in ΔH_{m2} for the two samples PBS7 and PBS8 with the highest molar masses, corresponding to the disappearance of the exothermic peak T_{cc} (Figure 3). On the one hand, this behavior means that the increase in molar mass up to 150,000 g mol^{-1} is an essential condition for the thickening of crystals. On the other hand, the presence of an exothermic peak is an essential condition for the formation and/or reorganization of thicker crystals.

Finally, as can be seen in Figure 6, for the samples where we noted the presence of a cold-crystallization, the enthalpy of melt-crystallization ΔH_c is always lower than the total enthalpy of fusion ΔH_{mt}. The difference between ΔH_{mt} and ΔH_c lies between 5 and 10 J g^{-1}, while the enthalpy of cold-crystallization ΔH_{cc} is mostly constant between 10 and 12 J g^{-1}. These results show that the presence of an exothermic peak T_{cc} is not only related to a reorganization/recrystallization of small and/or imperfect crystals. It also seems that a new crystalline phase, which had not been formed during the melt-crystallization, forms from the amorphous phase of PBS; in which case, there is also the classical cold-crystallization process before the fusion of a polymer. However, the disappearance of the cold-crystallization T_{cc} and the appearance of a new endotherm T_{m4} for the two last samples PBS7 and PBS8 (Figure 3) mean that the rate of melting predominates over that of crystallization. But from Figure 6, we also note that the enthalpy of melt-crystallization ΔH_c becomes higher than that of total fusion ΔH_{mt}. Therefore, we can assume that exothermic phenomena related to reorganization occur during the melting of these two samples. These thermal transformations will be detailed in the next part about Modulated Temperature DSC measurements.

MTDSC measurements. We performed measurements in MTDSC to highlight the effect of reorganization which occurs during the melting of PBS. These thermal phenomena were studied during the second heating scan. To illustrate these measurements, three thermograms (PBS1, PBS5, and PBS7) corresponding to the three groups mentioned above are represented in Figure 7. The Reversible (Rev), the Non-Reversible (Non-Rev) and the Total DSC signals are presented for each thermogram.

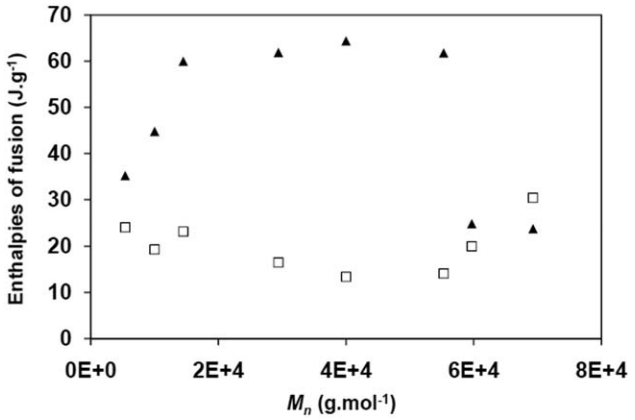

Figure 5. Enthalpies of fusion ΔHm_1 (□) and ΔHm_2 (▲) versus M_n of PBS.

First, we note that the profiles of the total signal of PBS1 and PBS5 are roughly the same as those with a heating rate of 10°C min^{-1} (Figure 3). However, an exothermic peak occurs before the melting peak on the total signal of PBS7. This new peak is situated at around 106°C, corresponding to the temperature of the endotherm T_{m4} (Figure 3). This means that PBS with the high molar masses can crystallize/reorganize when the heating rate is decreased.

Moreover, we observe the presence of a shoulder located at around 112°C on the melting peak, corresponding to the endotherm T_{m1} observed previously (Figure 3).

The reversible signal of the samples PBS1 and PBS5 reveals the presence of a dissimulated endotherm under the exothermic peak of the total signal (Figure 7). However, we note that the exothermic peak of the total signal occurs at a slightly lower temperature than the onset of the endothermic peak on the reversible signal. This difference is more pronounced for PBS1. This observation would suggest that this new crystalline phase is initially formed from the amorphous phase and not from the melting of imperfect crystals. The latter phenomenon likely occurs in a second step. Finally, we observe a reversible signal throughout the fusion of these two samples.

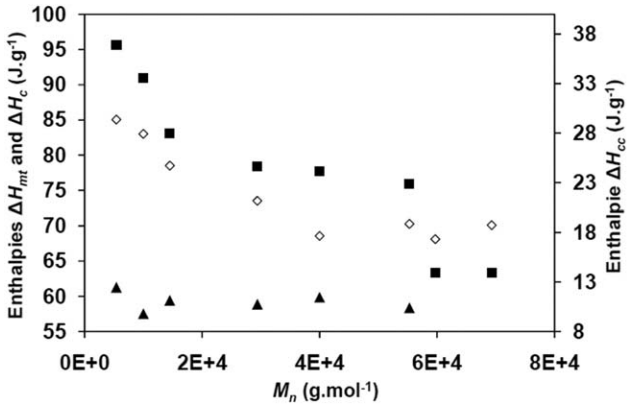

Figure 6. Total enthalpies of fusion ΔH_{mt} (■) and crystallization ΔH_c (◇) and enthalpy of cold-crystallization ΔH_{cc} (▲) versus M_n of PBS.

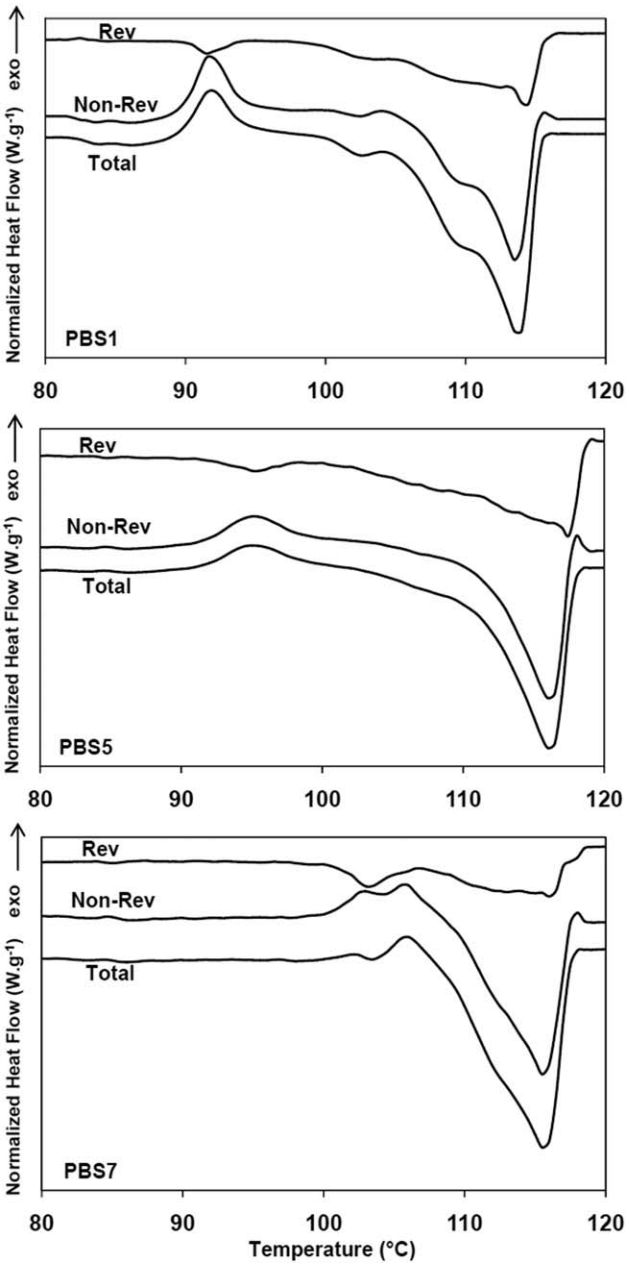

Figure 7. MTDSC thermograms with Reversible (Rev), Non-Reversible (Non-Rev) and Total signals of PBS samples chosen as examples of the three groups of thermograms. Heating rate of 1°C min^{-1}.

The behavior of PBS7 is slightly different from the two previous samples. The first endothermic peak, which occurs in the reversible signal at around 103°C, is more amplified than that of PBS1 and PBS5. Moreover, the onset of this peak is situated at a temperature similar to that of the occurrence of the exothermic peak on the non-reversible signal. As can be seen, a second exothermic peak occurs at around 106°C in the non-reversible signal while at the same time the first endothermic peak on the reversible signal ends. This results in the presence of an exothermic peak on the total signal. Thereafter, a reversible signal is observed throughout the melting of the sample.

In a study, Qiu et al.[27] showed the appearance of a crystallization exotherm between two endotherms in the total curve of MTDSC trace for a PBS with a 140,000 g mol^{-1} M_w mass. However, the experimental part showed that their measurements were carried out in *heat–cool* conditions, which favors the recrystallization of the macromolecules. Papageorgiou and Bikiaris[26] observed two well-distinguished recrystallization exotherms in the non-reversible curve of a PBS sample with a M_n of 6900 g mol^{-1}. Moreover, they also observed an enhancement in the reversing signal curve due to a continuous partial melting and crystal perfectioning through the fusion of PBS. However, they mentioned that the conditions of measurements and the low molar mass of the sample could ease the occurrence of a reversible signal. According to Wunderlich et al.[48–50] the reversible melting is due to a phenomenon of fusion-recrystallization of short macromolecular chains attached to a crystal with a higher melting temperature. This anchor crystal can be considered as a nucleation site for this short polymer segment. Moreover, this reversible melting is more pronounced in the imperfect crystals. According to Hu et al.[51] the sliding diffusion of the chains in the crystals is responsible for the force balance between the thinning and the thickening of the lamellae. This force balance causes a reversible surface melting and crystallization.

As can be seen in Figure 8, the measurement of the enthalpy of reversible melting ΔH_{rev} is not limited to PBSs with low molar masses. First, we can assume that the two first samples have a different mechanism of reorganization compared to the other samples. Indeed, we must remember that, for these two samples, all the exotherm and endotherms were situated at lower temperatures than for the rest of the series.

Then we observe a great decrease of ΔH_{rev} when the molar mass increases from 14,500 to 40,000 g mol^{-1}. Thereafter, we note a slight decrease in ΔH_{rev} with the increasing molar mass M_n. We can make two assumptions from these results: first, we can assume that for a certain molar mass (here 40,000 g mol^{-1}) the crystals of PBS are more stable and are less affected by the phenomenon of fusion-reorganization. Secondly, we can assume that the bigger the macromolecules, the more reduced the sliding diffusion effect of chains in crystals.

The Glass Transition of PBS. The glass transition temperature T_g of each sample was determined as the temperature at inflection point of DSC thermograms. T_g is located at around -32 ± 2°C for all samples. Contrary to the crystallinity, as can be seen in Figure 9(a), the heat capacity change ΔC_p in the glass transition region increases as the molar mass of PBS increases.

Like the evolution of crystallinity (Table II), we note a stabilization of ΔC_p when the molar mass reaches around 40,000 g mol^{-1} [Figure 9(b)]. However, this increase in ΔC_p is related to the difference in crystallinity of the samples studied. Indeed, as we observed above, the crystallinity of PBS decreases as molar mass increases, which means that, at the same time, the amorphous fraction increases. Menczel has reported the same behavior for poly(ethylene terephthalate) with various crystallinities: he observed an increase in ΔC_p as the crystallinity decreases.[52]

We observed a linear relationship between ΔC_p in the glass transition region, and the enthalpy of crystallinity ΔH_c of all

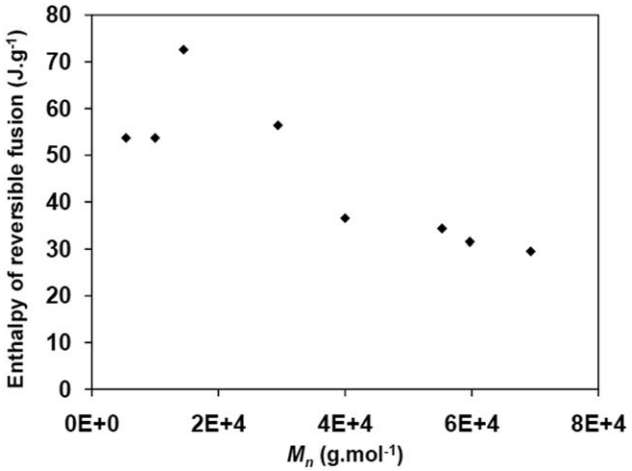

Figure 8. Enthalpy of reversible fusion ΔH_{rev} versus M_n of PBS.

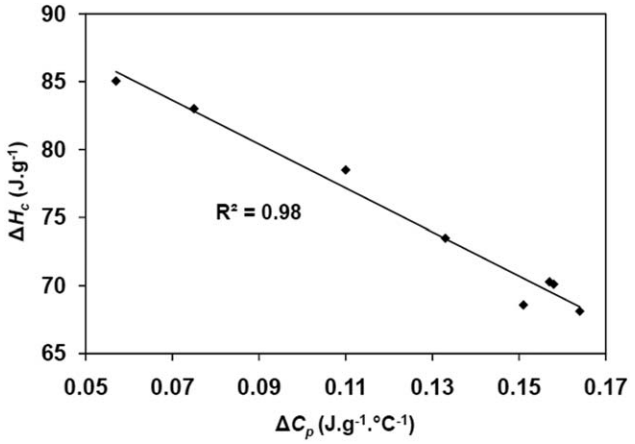

Figure 10. Enthalpy of crystallization ΔH_c versus heat capacity change ΔC_p during the glass transition of PBS.

samples (Figure 10). The linear fitting of this data gives us the following equation: $Xc = 47.5 - 80.8\Delta Cp$. Therefore, we can assume that an increase in X_c—and so a decrease in ΔC_p—should be observed, in the same experimental conditions used here, for a PBS sample with a lower molar mass, provided that the sample is a polymeric species. Also this relationship means that crystallinity of PBS samples studied here cannot excess 47.5% theoretically. In fact, the maximum X_c observed in this study is equal to 43% and corresponds to the sample PBS1 with the lowest molar mass: $M_n = 5400$ g mol^{-1}. For samples showing molar masses higher than the ones studied here, we can assume constant values of both X_c and ΔC_p, as observed for PBS samples with $M_n > 40{,}000$ g mol^{-1}. We did not find any reference mentioning this kind of behavior in literature. It would be interesting to confirm this linear relationship between X_c and ΔC_p with similar studies on different polymers.

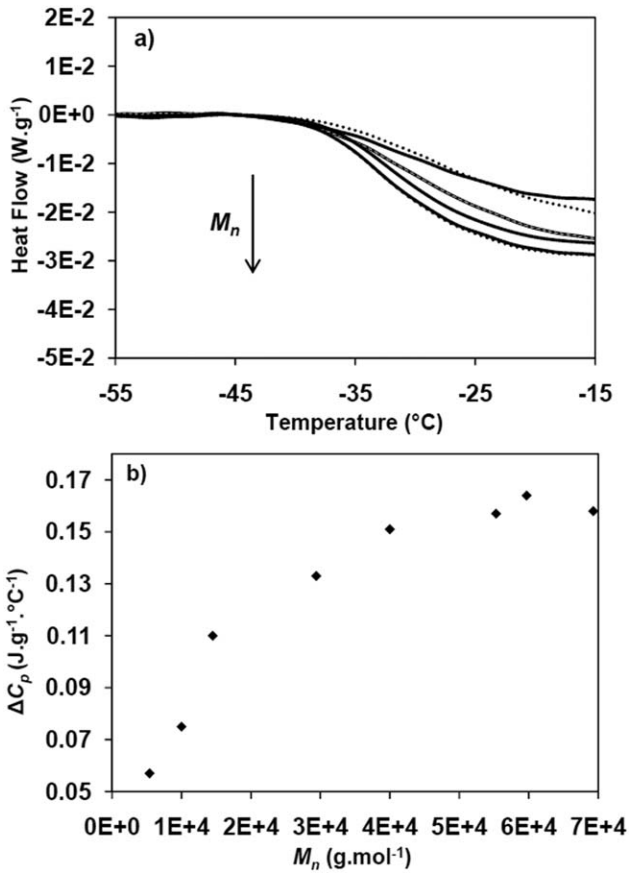

Figure 9. (a) DSC traces during the glass transition of different samples of PBS (for clarity reasons, curves were traced with solid lines or dashed points, so that all samples curves can be visible in this figure) and (b) the heat capacity change ΔC_p versus molar mass Mn of PBS.

CONCLUSIONS

The first objective of this study was to control the synthesis of high molar mass PBS by employing only the two monomers succinic acid and 1,4-butanediol. This has been achieved successfully as molar mass M_w of about 180,000 g mol^{-1} was reached in 6.5 h. The synthesis of high molar mass PBS follows the classical description of Flory theory on step-growth polymerization. Indeed, in the case of stoichiometric ratio of monomers, the kinetic rate constants were always higher than those of non-stoichiometric ratio. Moreover, we also observed an increase in kinetic rate constants when the amount of catalyst increased. However, in spite of a large amount of TBT, we noted a significant catalytic activity of the acid functions of succinic acid. This was attributed to a hydrolysis of TBT which decreases its catalytic activity. This result is in agreement with a recent study on the catalysts for the synthesis of PBS.[18]

The second part of this study dealt with the influence of molar mass on the thermal properties of PBS. First, the temperature and the rate of crystallization increase when the molar mass is superior to 60,000 g mol^{-1}. This behavior could be due to a memory effect of long macromolecules above the melting point. Secondly, we showed that the cold-crystallization T_{cc} before the fusion of PBS was also related to a transformation from amorphous phase to crystalline phase, as in classical cold-crystallization of polymers; and not only to the reorganization of crystals from imperfect to more stable. We demonstrated that the presence of T_{cc} is an essential condition for the formation of more stable crystals. Moreover, the MTDSC measurements

showed that, under our experimental conditions, a good stability of PBS crystals was reached from a molar mass of about 40,000 g mol^{-1}. This molar mass is also the starting point for a constant value of enthalpy of crystallization ΔH_c (70 J g^{-1}) and of heat capacity change during glass transition ΔC_p (0.16 J $g^{-1}{}^{\circ}C^{-1}$). Finally, we found a linear relationship between these two parameters, but it would be interesting to confirm the same kind of behavior for other polymers.

ACKNOWLEDGMENTS

This work has been financially supported by Conseil Régional Champagne-Ardenne, in the scope of the research project MATOREN, to whom the authors express their gratitude.

REFERENCES

1. Plastics Europe. http://www.plasticseurope.fr/Document/plastiques-2011-faits-et-chiffres.aspx?FolID=2 (Accessed Jul 3 2012).
2. European Bioplastics. http://en.european-bioplastics.org/market/ (Accessed Jul 3, 2012).
3. Amass, W.; Amass, A.; Tighe, B. *Polym. Int.* **1998**, *47*, 89.
4. Vroman, I.; Tighzert, L. *Materials* **2009**, *2*, 307.
5. Avérous, L.; Pollet, E. In Environmental Silicate Nano-Biocomposites, Avérous, L.; Pollet, E., Eds.; Springer London: London, **2012**, p 13.
6. Gupta, B.; Revagade, N.; Hilborn, J. *Prog. Polym. Sci.* **2007**, *32*, 455.
7. Auras, R.; Harte, B.; Selke, S. *Macromol. Biosci.* **2004**, *4*, 835.
8. Gupta, A. P.; Kumar, V. *Eur. Polym. J.* **2007**, *43*, 4053.
9. Maharana, T.; Mohanty, B.; Negi, Y. S. *Prog. Polym. Sci.* **2009**, *34*, 99.
10. Moon, S. I.; Lee, C. W.; Taniguchi, I.; Miyamoto, M.; Kimura, Y. *Polymer* **2001**, *42*, 5059.
11. Research and Markets. http://www.researchandmarkets.com/research/94lbkz/succinic_acid
12. Xu, J.; Guo, B.-H. In Plastics from Bacteria; Chen, G. G.-Q., Ed.; Springer Berlin Heidelberg: Berlin, Heidelberg, **2010**; Vol. *14*, p 347.
13. Xu, J.; Guo, B.-H. *Biotechnol. J.* **2010**, *5*, 1149.
14. Park, S. S.; Jun, H. W.; Im, S. S. *Polym. Eng. Sci.* **1998**, *38*, 905.
15. Bikiaris, D. N.; Achilias, D. S. *Polymer* **2006**, *47*, 4851.
16. Bikiaris, D. N.; Achilias, D. S. *Polymer* **2008**, *49*, 3677.
17. Hu, L.; Wu, L.; Song, F.; Li, B.-G. *Macromol. React. Eng.* **2010**, *4*, 621.
18. Jacquel, N.; Freyermouth, F.; Fenouillot, F.; Rousseau, A.; Pascault, J. P.; Fuertes, P.; Saint-Loup, R. J. Polym. Sci., *Part A: Polym. Chem.* **2011**, *49*, 5301.
19. Luo, S.; Li, F.; Yu, J.; Cao, A. *J. Appl. Polym. Sci.* **2010**, *115*, 2203.
20. Ahn, B. D.; Kim, S. H.; Kim, Y. H.; Yang, J. S. *J. Appl. Polym. Sci.* **2001**, *82*, 2808.
21. Han, Y.-K.; Kim, S.-R.; Kim, J. *Macromol. Res.* **2002**, *10*, 108.
22. Mochizuki, M.; Mukai, K.; Yamada, K.; Ichise, N.; Murase, S.; Iwaya, Y. *Macromolecules* **1997**, *30*, 7403.
23. Yang, J.; Zhang, S.; Liu, X.; Cao, A. *Polym. Degrad. Stab.* **2003**, *81*, 1.
24. Miyata, T.; Masuko, T. *Polymer* **1998**, *39*, 1399.
25. Papageorgiou, G. Z.; Achilias, D. S.; Bikiaris, D. N. *Macromol. Chem. Phys.* **2007**, *208*, 1250.
26. Papageorgiou, G. Z.; Bikiaris, D. N. *Polymer* **2005**, *46*, 12081.
27. Qiu, Z.; Komura, M.; Ikehara, T.; Nishi, T. *Polymer* **2003**, *44*, 7781.
28. Wang, X.; Zhou, J.; Li, L. *Eur. Polym. J.* **2007**, *43*, 3163.
29. Yoo, E. S.; Im, S. S. J. Polym. Sci., *Part B: Polym. Phys.* **1999**, *37*, 1357.
30. Yasuniwa, M.; Satou, T. J. Polym. Sci., *Part B: Polym. Phys.* **2002**, *40*, 2411.
31. Yasuniwa, M.; Tsubakihara, S.; Satou, T.; Iura, K. J. Polym. Sci., *Part B: Polym. Phys.* **2005**, *43*, 2039.
32. Cao, A.; Okamura, T.; Nakayama, K.; Inoue, Y.; Masuda, T. *Polym. Degrad. Stab.* **2002**, *78*, 107.
33. Nagata, M.; Goto, H.; Sakai, W.; Tsutsumi, N. *Polymer* **2000**, *41*, 4373.
34. Papageorgiou, G. Z.; Bikiaris, D. N. *Biomacromolecules* **2007**, *8*, 2437.
35. Xu, Y.; Xu, J.; Guo, B.; Xie, X. J. Polym. Sci., *Part B: Polym. Phys.* **2007**, *45*, 420.
36. Xu, Y.; Xu, J.; Liu, D.; Guo, B.; Xie, X. *J. Appl. Polym. Sci.* **2008**, *109*, 1881.
37. Nikolic, M. S.; Djonlagic, J. *Polym. Degrad. Stab.* **2001**, *74*, 263.
38. Tserki, V.; Matzinos, P.; Pavlidou, E.; Vachliotis, D.; Panayiotou, C. *Polym. Degrad. Stab.* **2006**, *91*, 367.
39. Ye, H.-M.; Wang, R.-D.; Liu, J.; Xu, J.; Guo, B.-H. *Macromolecules* **2012**, *45*, 5667.
40. Zhang, N.; Qu, J.; Tan, B.; Lu, X.; Huang, J.; Zhang, G.; Zhao, Y.; Jin, G. *J. Appl. Polym. Sci.* **2013**, *130*, 2544.
41. Menczel, J. D.; Judovits, L.; Prime, R. B.; Bair, H. E.; Reading, M.; Swier, S. In Thermal Analysis of Polymers; Menczel, J. D.; Prime, R. B., Eds.; John Wiley & Sons, Inc.: Hoboken, New Jersey **2008**, p 7.
42. Fradet, A.; Maréchal, E. *Adv. Pol. Sci.* **1982**, *43*, 51.
43. Ahmadnian, F.; Velasquez, F.; Reichert, K. H. *Macromol. React. Eng.* **2008**, *2*, 513.
44. Siling, M. I.; Laricheva, T. N. *Russ. Chem. Rev.* **1996**, *65*, 279.
45. Flory, P. J. *J. Am. Chem. Soc.* **1939**, *61*, 3334.
46. Odian, G. In Principles of Polymerization, 4th Edition; George Odian, Ed.; John Wiley & Sons, Inc.: Hoboken, New Jersey **2004**, p 39.
47. Rieger, J. In Polymer Crystallization; Reiter, G.; Sommer, J.-U., Eds.; Springer Berlin: Heidelberg, **2003**; Vol. *606*, p 7.
48. Okazaki, I.; Wunderlich, B. *Macromolecules* **1997**, *30*, 1758.
49. Pak, J.; Wunderlich, B. *Macromolecules* **2001**, *34*, 4492.
50. Pyda, M.; Wunderlich, B. *J. Polym. Sci., Part B: Polym. Phys.* **2000**, *38*, 622.
51. Hu, W.; Albrecht, T.; Strobl, G. *Macromolecules* **1999**, *32*, 7548.
52. Menczel, J. D. *J. Therm. Anal. Calorim.* **2011**, *106*, 7.